ACS NANO

www.acsnano.org

ARTICLE

Ionic Strength-Dependent Assembly of Polyelectrolyte-Nanoparticle Membranes via Interfacial Complexation at a Water–Water Interface

Wilfredo Mendez-Ortiz, Kathleen J. Stebe,* and Daeyeon Lee*

Cite This: https://doi.org/10.1021/acsnano.2c08916

Read Online

ACCESS | Metrics & More | Article Recommendations | Supporting Information

ABSTRACT: Complexation between oppositely charged nanoparticles (NPs) and polyelectrolytes (PEs) is a scalable approach to assemble functional, stimuli-responsive membranes. Complexation at interfaces of aqueous two-phase systems (ATPSs) has emerged as a powerful method to assemble these functional structures. Membranes formed at these interfaces can grow continuously to thicknesses approaching several millimeters and display a high degree of tunability via modification of solution properties such as ionic strength. To identify the membrane assembly mechanism, we study interfacial assembly in a prototypical dextran/PEG ATPS, in which silica (SiO_2) NPs suspended in the PEG phase undergo interfacial complexation with poly(diallyldimethylammonium chloride) (PDADMAC) supplied in the dextran phase. Using a microfluidic device that facilitates sequential insertion of fluorescent and nonfluorescent PDADMAC, we observe a transition in the membrane growth mechanism with ionic strength. In the absence of added salt ([NaCl] = 0 mM) PDADMAC chains permeate through the existing membrane to complex with NPs on the PEG side of the membrane, leading to the formation of well-stratified structures. At elevated ionic strength ([NaCl] = 500 mM), this permeation mechanism is lost. Rather, the complexing species incorporate uniformly across the membrane. We attribute this transition to a rapid exchange of PE-counterion, NP-counterion, and PE/NP binding sites facilitated by an increase in extrinsically compensated charged groups on the NPs and PEs at high salinity. These PDADMAC/SiO_2 NP membranes have tremendous potential for the formation of functional membranes, offering control over the internal structure and serving as an ideal system for the generation of targeted release systems.

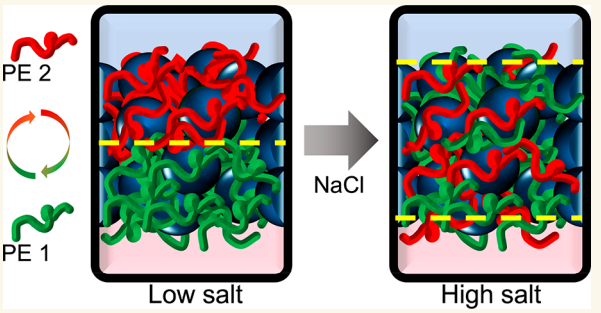

KEYWORDS: *Interfacial complexation, aqueous two-phase system, polyelectrolytes, microfluidics, coacervate*

INTRODUCTION

Complexation of charged species, including polymers, colloids, and surfactants at liquid–liquid interfaces, is a versatile technique to generate membranes with diverse functionalities. By exploiting the interaction between complementary species at an interface, microcapsules can be created for a variety of applications, including the targeted delivery of drugs,[1] the multiplexed sensing of species in solution,[2] and the fabrication of self-healing materials.[3] Furthermore, membrane formation by interfacial complexation is a highly scalable process.[4] Interfacial assembly schemes provide a complementary approach to the well-established membrane production method known as layer-by-layer (LbL) assembly, which is relatively time-consuming, typically requires a solid substrate to prime growth, and is limited to relatively thin films and membranes.[5]

Interfaces between aqueous and oil phases are widely exploited for membrane assembly. The differing polarity of these fluids allows selective solvation of membrane-forming components, and the elevated tension of their interfaces promotes adsorption and trapping of complexed species.[4−8]

Received: September 6, 2022
Accepted: November 17, 2022

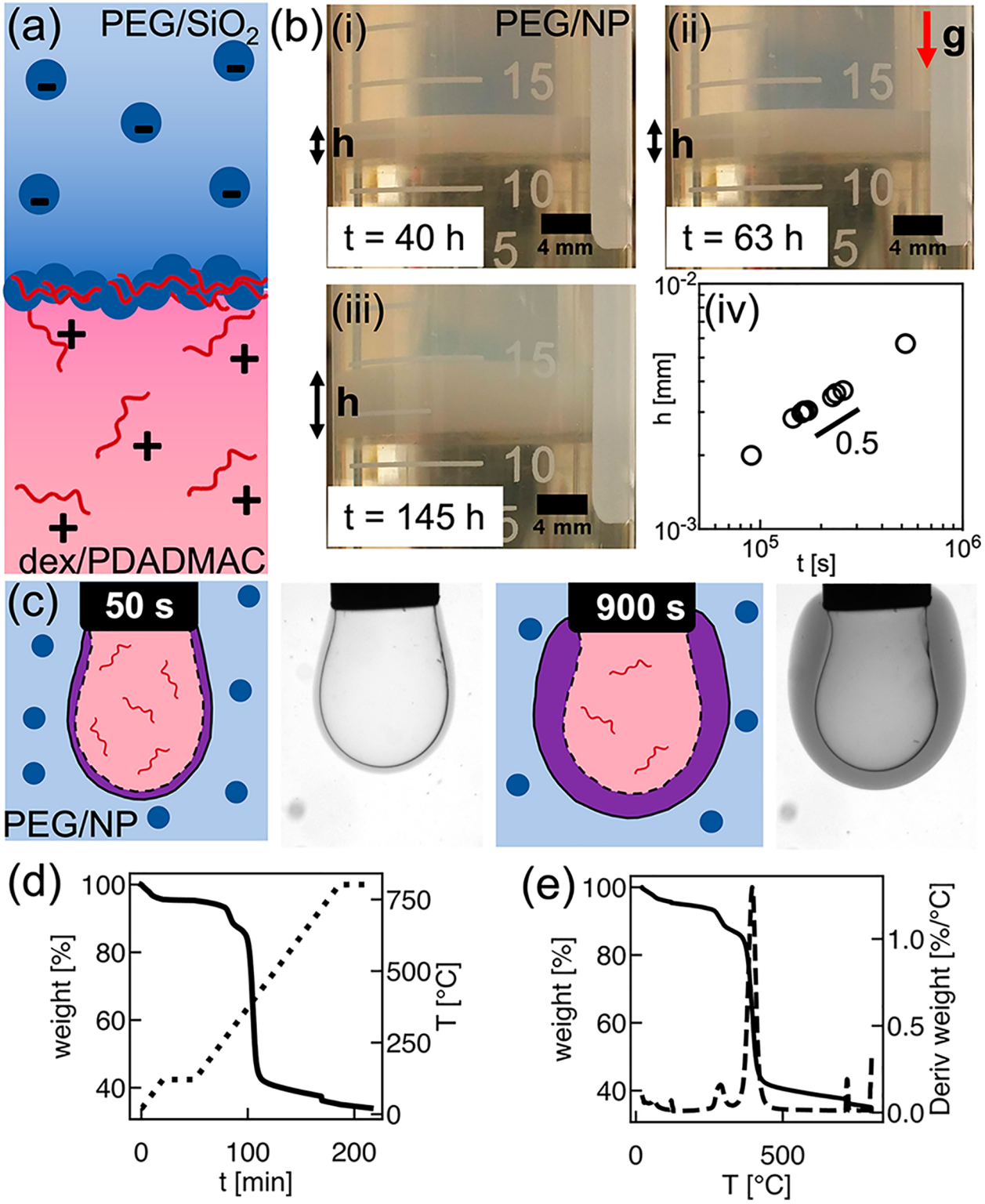

Figure 1. (a) Schematic of the interfacial complexation in an aqueous two phase system (ATPS) composed of dextran (450 000−600 000 g/mol) and poly(ethylene glycol) (20 000 g/mol). The complexing materials are the cationic polyelectrolyte poly (diallyldimethylammonium chloride) (PDADMAC) and the anionic SiO_2 nanoparticle (NP). (b) Growth of a 1.5 wt % PDADMAC/8 vol % SiO_2 NP interfacial membrane over 6 days with a final membrane thickness of 6 mm. (b i-iii) Time-lapse of membrane growth. (b-iv) Thickness evolution as a function of time, with a power-law growth rate with slope of 0.5. (c) Membrane formation on the interface of a pendant drop; a 1 μL, droplet phase composed of 15 wt % dextran/1 wt % PDADMAC at 100 mM NaCl is inserted at 1 μL/s into a continuous phase of 10 wt % PEG/4 vol % of SiO_2 NP at 100 mM NaCl. Needle OD is 0.9 mm. (d) Temperature ramp for thermogravimetric analysis (TGA) of a 15 wt % dex/5 wt % PDADMAC and 10 wt % PEG/4 vol % NP complexes. The solid line indicates weight percentage, and the dashed line indicates the process temperature. (e) Plot showing the thermal decomposition of PE/NP complexes. Solid line shows the mass evolution, and the dashed line shows the derivative of the weight with respect to temperature. The thermogravimetric analysis is performed under an inert nitrogen atmosphere.

https://doi.org/10.1021/acsnano.2c08916
ACS Nano XXXX, XXX, XXX−XXX

However, such interfaces may not be ideal for delicate materials such as living cells, proteins, and other biological entities, and the distinct polarity of each phase can constrain the palette of the membrane components. To overcome these challenges, we and others have exploited the interface formed in aqueous two-phase systems (ATPSs).[9−11] For example, complexation between oppositely charged species has been shown to arrest phase separation dynamics and lead to the formation of complexed membranes.[12−15] The ability to solvate complexing species in either phase can be exploited to influence the assembly process, for example, to favor interfacial complexation to generate microcapsules or to favor bulk complexation to generate microgels.[16,17]

While interfacial complexation of two oppositely charged polyelectrolytes (PE) in ATPS was first studied to prepare microcapsules,[10,18,19] this approach has since been exploited to generate tubular and multicompartmental structures attractive for multicompartment reactions and transport of species.[15,20,21] In principle, interfacial complexation in ATPS requires only that the components be charged and water-soluble, allowing tremendous flexibility in the selection of complexing materials and additional degrees of freedom in design of membrane functionality. For example, by simply swapping a PE for a nanoparticle (NP), complexed membranes can be formed with very different properties.[22] Membranes formed by PE/NP complexation differ in permeability from their PE/PE counterparts,[23] and NP can be selected to impart additional functionalities. For example, PE/NP membranes can exhibit high rigidity and permeability, can exchange materials across the membrane via osmotic fluxes, and can incorporate cargo by exploiting interactions with the charged species.[22−24] Furthermore, diverse multicompartmentalized structures can be formed, allowing selective segregation of cargo within the domains.[24]

While these studies demonstrate the tremendous promise of PE/NP membranes formed by interfacial complexation, the membrane growth mechanism in this process remains unknown. Most studies to date in ATPS have focused on the bulk dynamics that occur during the interfacial complexation process and have not delved deeply into the assembly mechanisms that determine membrane growth.[18,22,23] Mechanistic insights that relate interfacial complexation dynamics, membrane structure, and their dependence on solution properties would provide invaluable guidance in membrane design.

Although mechanistic studies for interfacial complexation in ATPS are lacking, film growth mechanisms have been elucidated in LbL systems, which rely on sequential adsorption of oppositely charged species on a solid support. Key concepts established in the LbL literature provide important guidance. LbL studies distinguish between two distinct types of binding whose probability of formation and rearrangement rate depend strongly on the ionic strength of the two solutions, PE molecular weight, and adsorption times.[25,26] Complexation can occur with binding of intrinsic sites, in which oppositely charged sites of complexing species meet, or by binding of extrinsic sites, in which charged sites on the complexing species interact with counterions in the film. High ionic strengths favor the formation of rapidly exchanged extrinsic binding sites that facilitate PE incorporation into LbL films and favor the so-called exponential growth or superlinear growth regime.[27]

To improve our understanding of the interfacial complexation process, we study the growth of interfacial membranes prepared via the complexation of cationic poly(diallyldimethylammonium chloride) (PDADMAC) and negatively charged SiO_2 NPs at the interface of the dextran and PEG phases. By employing a microfluidic device that allows sequential introduction of unlabeled and fluorescently labeled PDADMAC, the membrane assembly process is directly monitored. In the absence of added salt, the membrane growth is dominated by PE permeation across the membrane to meet uncomplexed NP on the far side of the membrane. This mechanism results in stratification within the membrane structure, with fresh membrane forming at the PEG/membrane interface. This stratified structure is eliminated as the salt concentration increases, promoting rapid exchange of both intrinsic and extrinsic bonds within the membrane. This rapid exchange of bonds ultimately leads to a homogeneous distribution of incorporated PDAMAC throughout the membrane. These salt mediated mechanisms give control over the spatial arrangement of PE within the membrane, providing an axis for the design of functional membranes with stratified or homogeneously loaded cargo via interfacial complexation. This finding suggests that charged functional species can be specifically positioned throughout the cross-section of the membrane, for example, to define films with multiple reaction zones or with selected regions that can be triggered by external stimuli.

RESULTS AND DISCUSSION

Growth and Thickening of PDADMAC and SiO_2 NP Interfacial Membrane in ATPS. We study the formation of PDADMAC/SiO_2 NP complex membranes (Figure 1a) as a model system to understand interfacial complexation at the ATPS interface. This system allows us to form stable capsules when a PDADMAC-containing dextran solution is electrosprayed into a bath of PEG with SiO_2 nanoparticles. Upon introduction of a droplet of one phase in a bath of the other phase, a rigid PDADMAC/NP membrane is formed at the interface of the ATPS, stabilizing a water−water emulsion.[23] We perform all studies of these assemblies with a low molecular weight (<100 000 g/mol) PDADMAC, assuring rapid stabilization and growth under approximately isotonic conditions (Figure S1).

To directly observe membrane growth, we induce complexation of PDADMAC and SiO_2 NP at a macroscopic, planar interface (Figure 1b). The interface is formed by mixing a dextran (15 wt %; 100 mM NaCl) solution, PEG (10 wt %; 100 mM NaCl) solution, and 22 nm SiO_2 (8% volume) NPs suspension in a 50 mL conical centrifuge tube and subsequently allowing this three component mixture to phase separate.[28,29] The phase separation generates a water−water interface which serves as the membrane assembly scaffold. During the phase separation process, SiO_2 NPs partition to the PEG phase (Figure S2). PEG is known to interact with the silanol groups via hydrogen bonding in a highly pH[30,31] and salt dependent manner.[32,33] Thus, this partitioning is driven by two complementary phenomena: favorable PEG/SiO_2 interaction and low affinity between dextran and SiO_2.[34,35] Membrane growth is initiated by introducing a PDADMAC-containing dextran solution while simultaneously withdrawing the dextran phase such that the interface is maintained at the same position. Once the PDADMAC is introduced, the dex/PEG interface is rapidly covered by a membrane that forms via the interfacial complexation of the PDADMAC in the dextran phase and the SiO_2 NPs in the PEG phase (Figure 1b,c). This

https://doi.org/10.1021/acsnano.2c08916
ACS Nano XXXX, XXX, XXX−XXX

membrane shows rapid and continuous growth over a six-day timespan, reaching a thickness of up to 6 mm.

The macroscopic membrane thickness $h(t)$ evolves as $h(t) \sim t^{1/2}$(Figure 1b(iv)). This scaling highlights the importance of diffusion in the membrane growth process; similar trends have been reported for interfacially grown membranes at oil−water interfaces.[36,37] The apparent diffusion coefficient estimated from this data is roughly 10^{-12} m^2/s. While this coefficient does not reflect the self-diffusivity of the complexing species in the membrane, it does reflect a growth process that relies on the incorporation of the two species. Notably, its value is comparable to the bulk diffusivities of NPs and PEs in the dextran and PEG solutions, assuming Stoke-Einstein and a gyration radius of 21 nm for PDADMAC (taken by interpolation from Dautzenberg et al.[38]). This indicates that components are incorporated rapidly, inducing the observed rapid membrane growth. Apparent diffusion coefficients of this magnitude have been reported previously for highly hydrated LbL PE/PE films;[27] which is likely the case for ATPS interfacial membranes.

Membrane growth at early times (<1 h) can be monitored *in situ* on the interface of a pendant drop (Figure 1c, Movie S1). At 100 mM NaCl, upon introducing a 1 wt % PDADMAC droplet phase into a continuous PEG/NP (4% per volume), the formation of a membrane at the dex/PEG interface is rapidly achieved. This is in marked contrast to previous reports of relatively slow membrane growth absent salt, as is shown in Figure S3.[23] In the presence of 100 mM NaCl, the membrane grows continuously, with a developing membrane front that moves in the direction of the PEG/NP bulk phase. (We consistently observe that, as the membrane thickens, it becomes attached to the outer needle wall; this is attributed to favorable wetting of the complexes at the solid surface.)

The growth of membrane fronts into one phase is commonly observed in ATPS-based interfacial membranes and has been attributed to the affinity of one or both complexing agents for a particular phase.[16,21] PDADMAC has been reported to have a slight preference for the PEG phase.[17] Moreover, strong partitioning of SiO_2 NP indicates that they also have a high affinity for the PEG phase (Figure S2). To understand the role of selective partitioning on membrane growth, we study membrane growth on pendant drops by swapping the locations of PDADMAC and SiO_2 NP. In these experiments, SiO_2 NPs are suspended in the internal dextran phase, and PDADMAC is present in the external PEG solution. Figure S4a,c and Movie S2 shows that, in this configuration, the membrane front grows inward toward the dex/NP phase, leading to the eventual formation of a drop-shaped microgel made of complexed PDADMAC and SiO_2 NPs. This result indicates that the membrane grows into the NP containing phase, regardless of the placement of the two species. This fast and directional growth of the membrane suggests that rapid PDADMAC diffusion within the membrane must play an important role in the membrane growth process. Additionally, we have observed that the membrane growth has some dependence on PDADMAC and NP concentration. Increasing PDADMAC concentration leads to increases in the membrane growth rate, whereas increasing the NP concentration has the opposite effect. These trends may be attributed to the important role played by PDADMAC diffusion within the membrane. Higher PE concentration increases the PE flux, whereas greater NP density impedes PE diffusion.

This fast growth suggests that the membrane is highly porous and swollen with water rather than being densely packed with solid nanoparticles which would significantly impede the diffusion of PDADMAC. The membrane composition is characterized using a thermogravimetric analysis (TGA) (see SI for a detailed description of the membrane growth for TGA; Figure S5). In TGA, the temperature (T) is ramped at a rate of 5 °C/min from 21 to 120 °C; T is then held constant at 120 °C for 30 min. Thereafter, T is ramped once again to 800 °C at 5 °C/min, and then held fixed at 800 °C for 30 min. From the thermogram and its derivative in Figure 1e, two main mass change events are observed. The first peak in the derivative of the weight loss takes place around 288 °C. This indicates the removal of PDADMAC species from the membrane, which is close to the first decomposition peak of pure PDADMAC (314 °C) as shown in the Figure S6a. The second large mass removal event takes place around ∼396 °C, which correlates with both the PEG decomposition (396 °C) (Figure S6b) as well as the second peak (∼441 °C) for PDADMAC decomposition (Figure S6a). As reported in our prior work and as shown in Figure S7d, PEG has a tendency to cross the membrane, explaining its presence in the membrane and its impact on the TGA analysis. Additionally, PEG interacts with the NPs, through hydrogen bonding interaction; thus, some of the PEG TGA signatures in the membrane are likely from PEG adhered to SiO_2 NPs. Based on the TGA result, 67% of the total mass is attributed to the polymeric species, including PEG, PDADMAC, and dextran (Figure 1d,e). This implies that the solid NPs constitute the minor phase of the membrane and that these structures likely have ample spacing between NPs that are filled by the polymeric species and water.

Role of Salt and the Tunability of the Membrane Complexes. The importance of ionic strength on the complexation of various PE/PE or PE/NP pairs is well-documented; ions can modulate electrostatic interactions between species, the transport of polyelectrolytes, and the molecular structure of complexes.[39,40] To understand the effect of NaCl on the interfacial complexation of PDADMAC/SiO_2 NP, a pendant drop experiment is executed in which the concentration of NaCl is increased isotonically in the two phases (Figure 2 and Movies S1 and S4). These isotonic conditions are defined to minimize the osmotic fluxes that would confound our results. At 0 mM NaCl, no additional counterions are added to the system, and intrinsic compensation between the PE and NP results in a thin

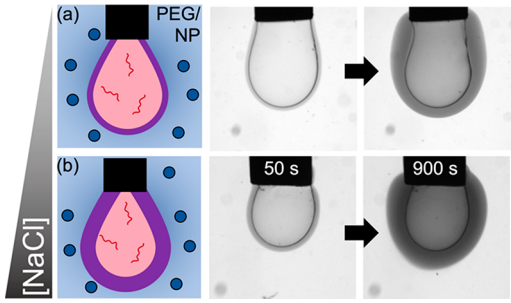

Figure 2. Effect of NaCl on the interfacial complexation. (a) Pendant drop assembly at 100 mM NaCl of a droplet phase composed of dex (15 wt %)/PDADMAC (1 wt %) on a continuous of PEG (10 wt %)/NP (4% vol.). (b) Pendant drop assembly of same conditions as (a) but at a 500 mM NaCl concentration.

https://doi.org/10.1021/acsnano.2c08916
ACS Nano XXXX, XXX, XXX−XXX

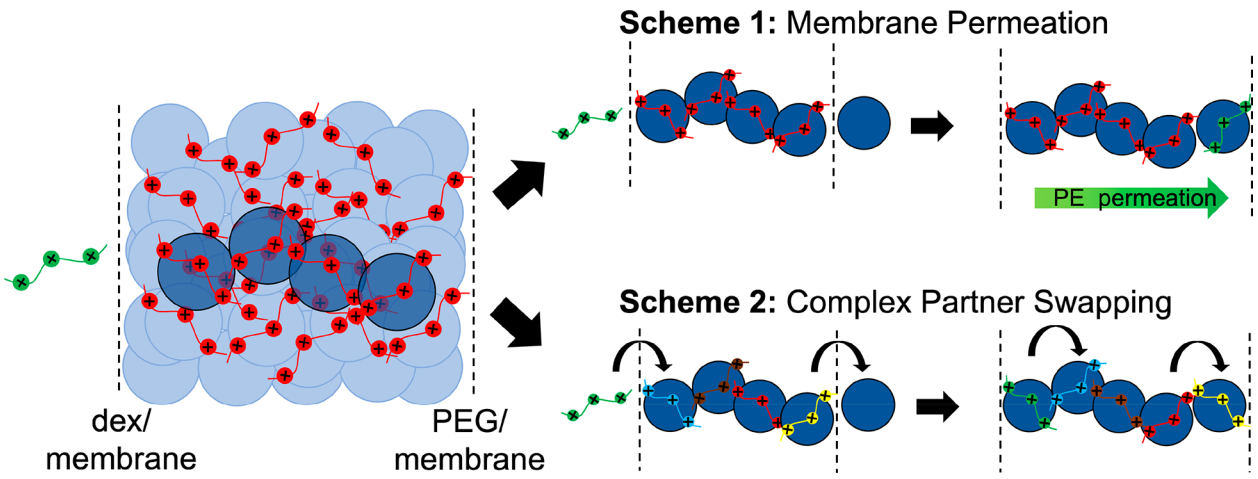

Figure 3. Proposed mechanisms for the interfacial growth of polyelectrolytes (PEs) and nanoparticles (NPs) in an aqueous two-phase system (ATPS). Scheme 1 (membrane permeation) is a scheme in which uncomplexed PEs permeate through the membrane thickness and undergo complexation with NPs at the membrane/PEG interface. In Scheme 2 (complex partner swapping), labile binding between the PE and NPs lead to a high degree of association and dissociation events throughout the membrane.

membrane at the interface (Figure S3). This process resembles our prior work,[23] in which a rigid membrane developed at the interface, and significant PEG exchange occurred between the two bulk phases. By adding an excess of counterions (Figure 2), a pronounced "thickening" of the membrane occurs, with an apparent faster growth rate for the higher salt concentrations (Figure 2b). Similar salt-mediated increases in membrane growth rates have been previously reported for PE/PE systems assembled in ATPS.[41]

Growth Mechanism for Interfacial Assembly of PDADMAC/SiO_2 NP. The growth of a PDADMAC/SiO_2 NP membrane at the interface of the ATPS strongly depends on the capacity of PEs to move within the membrane. Consider a cross-section of the membrane, a complex environment composed of multiple binding sites. Incoming PEs diffuse toward the PEG phase that contains SiO_2 NPs while interacting with unbound charged groups of SiO_2 NP within the membrane. Simultaneously, complexed PEs exchange their partners by dynamically unbinding and binding with multiple SiO_2 NPs within the membrane. This interplay between diffusion of the PE and the complexation reaction are the two primary factors that determine the membrane growth mechanism.

Motivated by the findings in the growth of LbL films, we propose two distinct growth schemes, based on the extent of complexation experienced by an incoming, initially uncomplexed PE. Complexation between a PE/PE and a PE/NP is a highly entropic process, mediated by the entropy gain from the counterion and water molecules upon complexation process.[42] This charge driven interaction is highly dependent on the molecular structure of the PEs with increasing blockiness (periodicity of monomer units) leading to a larger entropic drive for coacervation.[43] When the charged groups are intrinsically compensated (i.e., anionic groups of SiO_2 are compensated by the cationic groups of PDADMAC), the PE/NP interaction is "tight", with many repeat units wrapping around NPs. For the membrane to grow under these conditions, uncomplexed PDADMAC likely has to traverse the membrane to complex with free SiO_2 NPs on the far side of the membrane. This growth mechanism implies that the time scale for the dissociation between the cationic groups of PDADMAC and the anionic group of the NP is large, thus limiting the capacity of PDADMAC to diffuse after complexation. In this limit, therefore, there are two populations of PE; a population of nearly immobilized PE complexed to NP and a population of highly mobile uncomplexed PE that diffuses through the membrane. It is this latter population that, upon crossing the entire membrane, complexes with NP on the far side. We call this the membrane permeation scheme (illustrated in Figure 3), and it describes membrane growth at the limit of high intrinsic binding and low on−off binding ratio between the PE/NP complexes.

In the opposite limit, the on−off rate between the PE/NP is high, and the interactions between the two species are labile. These labile interactions allow PDADMAC chains that are bound to SiO_2 NPs to dissociate and to bind to other NPs within the membrane, effectively swapping NP binding partners (complex partner swapping scheme). This exchange allows PE that are entering the membrane to bind locally to unoccupied sites on NP made available by the rapid on−off kinetics. Thus, rather than two populations of PEs with highly differing mobility, the fast on−off kinetics allow PEs to migrate rapidly throughout the membrane. This mechanism is related to the self-exchange and site-diffusion mechanism found in PE/PE LbL films, where the addition of intrinsic charges (i.e., PEs) are accommodated by "defect" rearrangements through the film's cross section. In a typical LbL assembly, intrinsic charges are added at the growing interface of the film, whereas in PE/NP interfacial complexation, the PE enters the membrane at the opposite interface. For growth to occur in this arrangement, PEs within the membrane must rearrange to free up charged sites on NPs to interact with incoming PEs. Thus, for PE/NP interfacial complexation, PE diffusion plays an essential role in the growth of interfacial assemblies.

These mechanisms represent two limits of membrane assembly, in which the dynamics of association and disassociation between PE and NP determine how PEs transport within the membrane. One key parameter that has been omitted in this discussion is the role of extrinsic charges, i.e., added salts, and how these ions modulate the transition between these two growth limits. We hypothesize that the ionic strength of the solution serves as the key parameter that

https://doi.org/10.1021/acsnano.2c08916
ACS Nano XXXX, XXX, XXX−XXX

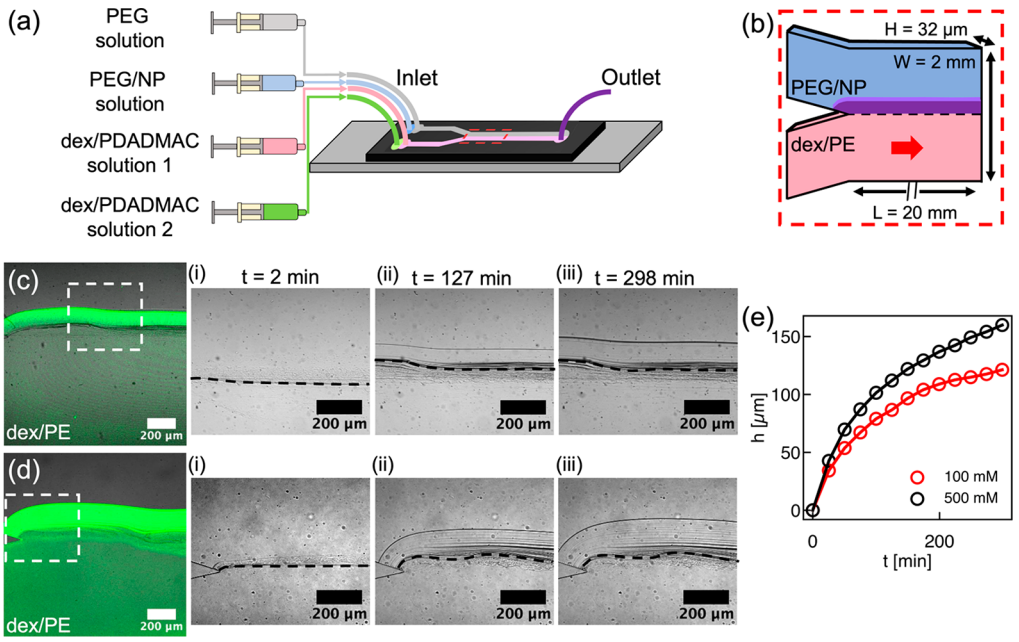

Figure 4. (a) Schematic of the microfluidic platform designed to probe the membrane assembly mechanism. The device contains four inlets and one outlet. The inlets allow continuous flow of PEG/NP and sequential insertion of dex/PDADMAC from fluorescently labeled or unlabeled streams. (b) Schematic of the inlet portion of the Y junction. The PEG/NP phase is introduced in the upper channel; the dex/PDADMAC is introduced in the bottom channel, both under continuous flow. (c) Interfacial membrane grown using dex/PDADMAC (2 wt %) and PEG/NP (4% vol.) after ~6 h. (i-iii) Time-lapse of membrane growth. (d) Interfacial membrane at dex/PDADMAC (2 wt %) and PEG/NP (4% vol.) after ~6.6 h. (i-iii) Time-lapse of membrane growth. (e) Plot showing thickness change as a function of time for c and d.

determines the mode of membrane growth.[44] Salt, through direct disruption of the pair interactions between the PDADMAC repeat unit and the SiO_2 NP, can control the association/dissociation dynamics of the two species.

The observed dependence of membrane growth rate on the ionic strength shown in Figure 2 does not discriminate between the two mechanisms. Either mechanism could be consistent with the observed increase in growth rate either via a direct increase in the diffusional transport due to the salt or via an increase in the dissociation rate as the ionic strength is increased. Thus, far, the methods we have used to study the membrane growth, including macroscopic growth and pendant drop studies, do not provide the necessary resolution to discern the growth mechanism.

Interfacial Assembly under Flow: Microfluidic Platform. To directly monitor membrane growth under well controlled conditions and steady concentrations of PDADMAC and SiO_2 NP, we devise a microfluidic platform as illustrated in Figure 4a and b. This platform has three important features. First, the microfluidics device allows continuous and sequential introduction of complexing species in two flowing streams, one of dextran/PE and the other of PEG/NP, and the formation of an interface between these streams. This obviates depletion effects and allows us to observe the membrane assembly over extended time periods. Second, the device allows *in situ*, real time observation of the membrane as it evolves at the interface. Third, the microfluidics study allows us to probe the spatial arrangement of these species as they complex at the aqueous−aqueous interface via fluorescence microscopy. These observations provide insight into the assembly mechanism and its dependence on ionic strength.

In this device, streams of PEG/NP and dex/PDADMAC meet at a Y-junction, and flow parallel to each other through a 20-mm-long channel, forming an interface between them. The convective flow continuously supplies PDADMAC and SiO_2 NPs, allowing us to monitor growth over extended timespans. These two species are able to diffuse orthogonally to the flow direction and undergo complexation at the interface between the two streams. We find that stable membrane growth can be induced by setting the width and height of the channel at 1 mm and ~32 μm, respectively.[45,46]

The experiment to form an interfacial membrane is implemented in two steps. The first step involves the formation of a steady interface by exposing a nanoparticle-free PEG solution to a dex/PDADMAC solution. These two phases are immiscible and thus generate a clean interface along the length of the Y-junction channel, whose position can be adjusted by varying the flow rates of the two streams. Thereafter, in step two, the PEG solution is replaced with a PEG/NP solution. By matching the shear stress at the interface via careful tuning of the flow rates, a steady membrane can be grown at the interface (Figure S8).[46] The flow rates used for these experiments are summarized in Table S1.

Immediately after introduction of the NP suspension, we observe the formation of a membrane at the interface (Figure 4c and d, Movie S5 and S6). We call this initial membrane "the primer membrane" which provides a robust layer onto which the subsequent membrane growth can take place. However, this layer also presents a physical barrier between the two species. In order for PDADMAC and NP to undergo complexation, PDADMAC has to enter the membrane and interact with the NPs. The growth rate of the membrane in the microfluidic setup, directly characterized through the transmission channel of a confocal microscope, is reported for NaCl concentrations of 100 mM and 500 mM in Figure 4c-e. The membrane growth rate for both conditions declines as a

https://doi.org/10.1021/acsnano.2c08916
ACS Nano XXXX, XXX, XXX−XXX

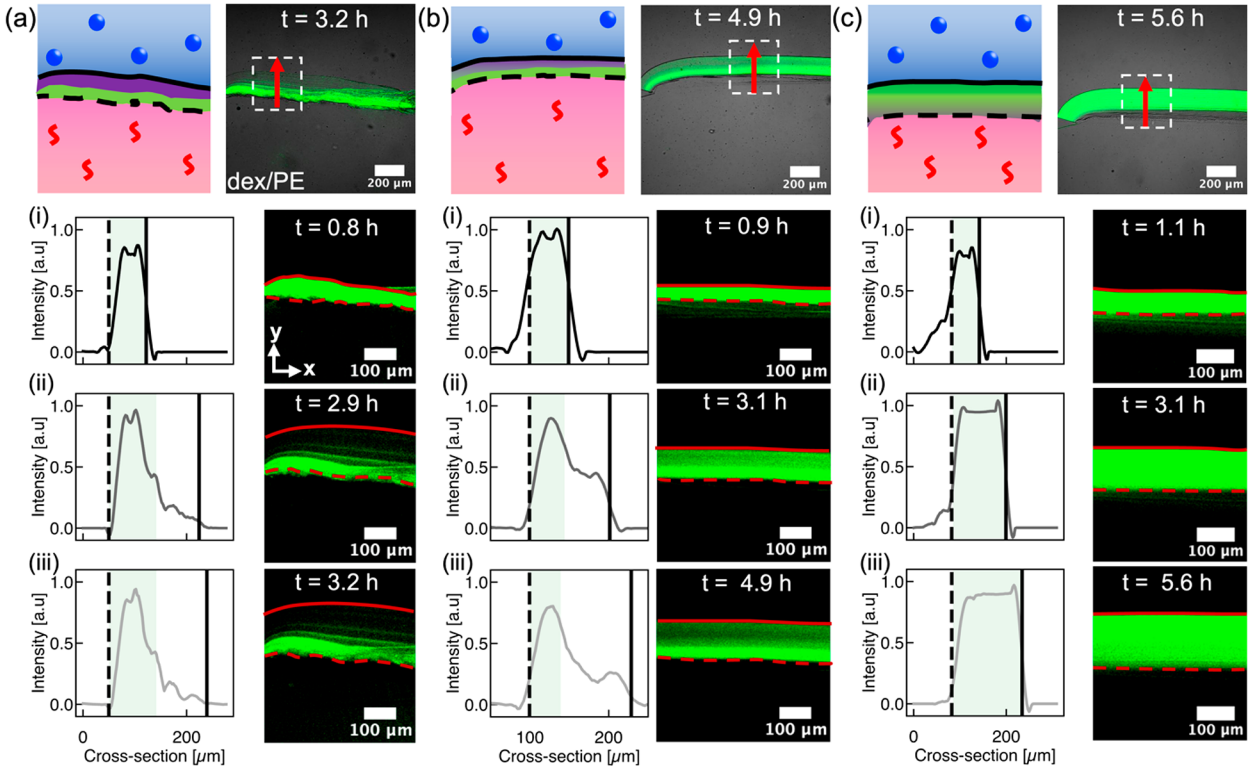

Figure 5. Summary of fluorescence evolution for two insertion events at [NaCl] = 0 mM, 100 mM, and 500 mM. (a i-iii) Fluorescence profile of the fluorescent channel for a double insertion event at 0 mM NaCl. A continuous stream of fluor-PDADMAC is exposed to a PEG/NP stream. Flow rates: 2 μL/min dex/PDADMAC and 19 μL/min PEG/NP. Fluorescent growth is for 45 min, after which point the fluorescent dex/PDADMAC stream is swapped for a nonfluorescent dex/PDADMAC stream. This nonfluorescent flow is sustained for 196 min. The dashed and solid line represent the dex/membrane and PEG/membrane fronts, respectively, which are determined from the transmission channel. The green area in the fluorescent profile represents the region at which the fluorescent band is present, measured directly from the fluorescent channel image. (b i-iii) Fluorescence profile for a double insertion event at 100 mM NaCl. Flow rates: 3.5 μL/min dex/PDADMAC and 19 μL/min PEG/NP. Fluorescent growth is for 48 min, after which point the fluorescent dex/PDADMAC stream is swapped for a nonfluorescent dex/PDADMAC stream. This nonfluorescent flow is sustained for 294 min. (c i-iii) Fluorescence profile for a double insertion event at 500 mM NaCl. Flow rates: 3.5 μL/min dex/PDADMAC and 19 μL/min PEG/NP. Fluorescent growth is for 48 min, after which point the fluorescent dex/PDADMAC stream is swapped for a nonfluorescent dex/PDADMAC stream. This nonfluorescent flow is sustained for 336 min.

function of time due to the innate hindering of the diffusion of PDADMAC as the membrane grows.

The interfacial assembly observed in the microfluidic device reveals some interesting features. For example, curved striations are observed in the membrane, and these curves become more tightly packed the farther away they get from the PEG/NP interface. We attribute these striations to pinning/depinning of the growing membrane on the top and bottom surfaces. We also observe that small features around 30 μm, presumably coacervate aggregates of PDADMAC and SiO_2 nanoparticles, detach from the growing membrane and flow away; however, these events do not seem to significantly impact the growth of the interfacial membrane and mostly take place at initial times, when the membrane is starting to form. Additionally, the membranes grown on the microfluidic device are always curved close to the entrance, where the pinning point is located. This curve stems from the complexes' favorable wetting of the PDMS surface, causing them to hug and thicken close to the wall. This is inevitable, since once the membrane grows away from the water−water interface it will interact with the wall and grow. Similar surface interactions are seen in the pendant drop as described previously (Figure 1c and Figure 2).

Stable interfacial membrane growth proceeds via complexation between PDADMAC and SiO_2 NPs which are continuously supplied in the flowing streams. This configuration circumvents one of the primary limitations imposed by other growth techniques such as electrospray and tubular formation in which the concentrations of the two species are changing during membrane assembly. In these methods, depletion of either or both complexing species leads to an eventual halt in the membrane growth.

The ionic strength of the solution also has an important effect on the growth rate. Thicker complexes develop at the interface of the pendant drop when increasing the solution NaCl concentration as shown in Figure 2. The microfluidic platform enables investigation of the effect of salt on the growth of these membranes in a more controlled setting. We can track membrane growth from its inception, track for longer times (>100 min), and prevent any instabilities of the NP suspension or reactant depletion. Additionally, these membranes are grown using dialyzed PDADMAC, which imposes a tighter MW distribution on the PDADMAC, limiting the effects of the inherently polydisperse stock solutions. The PDADMAC solution is dialyzed for 3 days, lyophilized, and then resuspended into a 15 wt % stock solution. Gel permeation chromatography data (Figure S9 and Table S2)

https://doi.org/10.1021/acsnano.2c08916
ACS Nano XXXX, XXX, XXX−XXX

show that the dialyzed PDADMAC has an average molecular weight of 29 377 g/mol, with a polydispersity index (PDI) of 1.59. The solution employed for these membranes includes a small portion of the PDADMAC that is labeled with Rhodamine (MW = 33 123 g/mol). Figure 4c and d show the growth for two interfacial membranes at different NaCl concentrations, grown for 5 h. During these 5 h, the growth is continuous and the membrane assembled at 500 mM has a faster growth rate than the one assembled at 100 mM as shown in Figure 4e.

Sequential Insertion: Capturing the Growth Mechanism. The microfluidics device facilitates the sequential introduction of different species and the *in situ* observation of their incorporation in the interfacial membrane. By alternating between two PDADMAC solutions, one of which is fluorescently labeled, the spatial location of the fluorescent PDADMAC (fluo-PDADMAC) can be visualized, providing important insights into the membrane growth mechanism. We perform such an experiment. Specifically, the dex/PDADMAC stream contains 15 wt % dex/2.00 wt % nonfluorescent PDADMAC. The dex/fluo-PDADMAC stream has similar composition, with 25% vol. of the nonfluorescent PDADMAC replaced with fluo-PDADMAC. The two PDADMAC populations share a similar lower bound MW, ~15 000 g/mol, imposed to minimize any PE diffusion effects due to the presence of small molecular weight species. Even though the two polymer samples have a broad range of molecular weights, their distributions are relatively similar, likely minimizing any impact the molecular weight may have on the growth of the membrane.

Membrane growth is initiated by flowing a PEG/NP stream in one channel and a dex/fluo-PDADMAC stream in the other. A membrane immediately forms at the interface and exhibits a high fluorescence intensity due to the incorporation of fluorescent PDADMAC. This membrane is allowed to grow for 40 to 45 min, after which, a nonfluorescent PDADMAC stream is introduced. The location of the nonfluorescent PDADMAC, as it is incorporated into the membrane, is monitored using the fluorescent and transmission channels simultaneously at different salt concentrations (Figure 5).

Absent added salt (0 mM NaCl), the original fluorescent band remains intact and maintains its initial position, with growth of nonfluorescent membrane occurring exclusively at the membrane/PEG interface (Figure 5a, Movie S7). This growth behavior is also evident in the fluorescence intensity profile across the membrane as a function of time, as reported in Figure 5a (i-iii). The intensity profile is measured for the initial membrane in the region spanned by the red arrow in Figure 5a immediately upon switching from the dex/fluo-PDADMAC to the dex/PDADMAC stream. In Figure 5a (i), the intensity profile shows low intensity outside of the membrane in the dex/PDADMAC phase, a peak of roughly uniform fluorescence of width ~72 μm, and a steep decrease in fluorescence intensity in the PEG/NP phase. Approximately 2.1 h later (Figure 5a (ii)), the membrane thickness has increased significantly to ~174 μm; however the location and shape of the fluorescence peak remain fixed. Even after 2.4 h have elapsed (Figure 5a (iii)), the initial fluorescence band remains intact, although a small broadening in the peak width has occurred (92 μm). These observations indicate that the membrane grows in a highly stratified manner and assembly occurs by the membrane permeation mechanism (Scheme 1 in Figure 3).

We perform a similar experiment with a salt concentration of 100 mM NaCl added equally to both phases. As in the previous case, we form an initial membrane that incorporates fluo-PDADMAC. The initial membrane is highly fluorescent (Figure 5b, Movie S8) with a steep fluorescence profile (Figure 5b (i)) and a total thickness of ~50 μm. 2.3 hours after introduction of the nonfluorescent PDADMAC stream, the membrane thickness has increased to ~129 μm. However, the fluorescence peak is now bimodal, with a visible bright band (40 μm) closer to the dex/membrane interface and a band of reduced fluorescence closer to the PEG/membrane interface. This configuration shows a weakening of membrane stratification in comparison to the 0 mM case.

At high salinity (500 mM NaCl), the distribution of the fluorescence signal in the film is dramatically altered, as shown in Figure 5c and Movie S9. We again form an initial membrane that incorporates the fluo-PDADMAC and switch to the nonfluorescent PDADMAC stream. Over time, the membrane thickens with a uniform fluorescence intensity profile; the stratified growth apparent at lower ionic strength is lost. After 4.5 h of continuous nonfluorescent PDADMAC insertion the membrane still maintains a homogeneous fluorescent distribution. This marks a clear change in the membrane assembly mechanism, indicating facile exchange of binding sites and high PDADMAC mobility within the membrane, as in the complex partner swapping scheme (Scheme 2).

In summary, as the ionic strength increases, the membrane growth mechanism and membrane structure change substantially. When the binding between the PE and NP is tight due to extensive intrinsic compensation between the two species at low ionic strength (<100 mM), the membrane grows by newly added PDADMAC traversing the existing membrane to complex with free SiO_2 NPs at the opposite membrane/PEG phase interface, as shown in the permeation scheme (Scheme 1 of Figure 3), leading to a stratified structure. As more salt is added to the system, rapid exchange of PE/NP binding sites allows PDADMAC to move freely within the membrane, thus generating a homogeneous membrane, as shown in the complex partner swapping scheme (Scheme 2 of Figure 3).

Building Stratified Membranes. Stratified membranes which have multiple layers of different composition and properties have a myriad of applications in reactive separation, actuation, sensing, and targeted delivery of materials among others. We demonstrate that interfacial complexation in ATPS can be used to build such membranes. We generate a membrane with four clearly distinct regions of alternating fluorescence intensity by flowing fluo-PDADMAC, PDADMAC, fluo-PDADMAC, and PDADMAC sequentially. Due to very tight binding between the NP and PE at low ionic strength, the membranes prepared under this condition have well-defined regions, with minimal intermixing between the four strata (Figure 6a, Movie S7). When the PDADMAC is switched four times at 100 mM NaCl (Figure 6b, Movie S8), we observe only weak stratification; the boundary between the three apparent regions is not very sharp and there is a weakened gradient in the fluorescence intensity. This is a potentially powerful method of controlling the internal structure of interfacial membranes. Depending on the intended application, it may be necessary to control the sharpness of the boundary between different strata, which can be easily tuned by ionic growth conditions.

https://doi.org/10.1021/acsnano.2c08916
ACS Nano XXXX, XXX, XXX−XXX

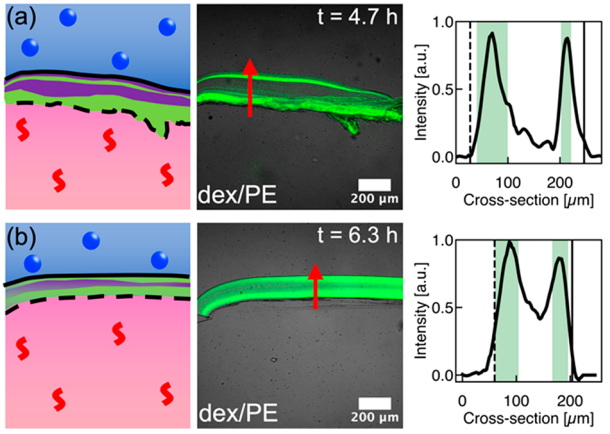

Figure 6. Fabrication of stratified membrane. (a) Four insertions at 0 mM NaCl. First fluorescent insertion was for 45 min, followed by nonfluorescent growth for 144 min. This is followed by a fluorescent and nonfluorescent insertion for 30 and 60 min, respectively. The plot shows the fluorescence profile through the cross-section of the membrane. (b) Four insertions at 100 mM NaCl. First a fluorescent insertion is performed for 48 min, followed by a nonfluorescent growth for 249 min. This is repeated once again for 30 and 51 min, respectively. Plot represents the intensity profile across the membrane. In both plots the dashed line represents the dex/membrane interface while the solid line represents the PEG/membrane interface. The green shaded portions represent the regions with fluorescent growth, measured from the images.

CONCLUSION

We have shown, through sequential insertion of PE species in a microfluidics platform, that the growth of membranes formed via interfacial complexation between PDADMAC and SiO_2 NPs at a water−water interface depends strongly on the ionic strength of the solution. At a low ionic strength, the membrane grows by the permeation of PDADMAC from the dex/PDADMAC phase through the existing PDADMAC/SiO_2 NP membrane to complex with NP at the interface of the PEG/SiO_2 NP phase. The permeation-based growth affords spatial control over the internal structure of the membrane, enabling incorporation of various composition and functionality into different strata. We have shown that distinct domains can be produced, and that the sharpness of the boundary can also be varied by increasing the ionic strength of the solutions. Stratified domains become more diffuse as ionic strength of the solutions is increased and are completely eliminated by PE intermixing at high ionic strengths. This understanding of the salt-dependent growth mechanism provides valuable control over the internal structure of the membrane.

The transitions in membrane assembly mechanisms discussed in this paper should spur additional fundamental studies to improve our understanding of interfacial complexation process. For example, knowledge of the association/dissociation rates of complexing species as a function of ionic strength from single molecule methods or simulations would provide valuable fundamental insight. In addition, quantitative measures of the diffusion coefficient within the complexed structure using techniques such as fluorescence recovery after photobleaching (FRAP) would provide important insights into the dynamics of structural rearrangements. On-going studies are focused on understanding the effect of growth conditions (ionic strength) and internal structuring (stratified vs homogeneous) on the macroscopic properties of the membranes such as permeability and mechanical robustness.

EXPERIMENTAL SECTION

Materials. All chemicals were purchased from Sigma-Aldrich unless otherwise noted. The biphasic ATPS system is based on poly(ethylene glycol) (PEG, MW = 20 000 g/mol) and dextran (dex, MW = 450 000−600 000 g/mol). Polycations used include poly(diallyldimethylammonium chloride) (PDADMAC, 35 wt % MW < 100 000 g/mol) and rhodamine tagged PDADMAC (1 mg/mL MW > 15 000 g/mol) from Surflay; average MW is obtained from the suppliers. In addition, PDADMAC solutions with MW ranging from 14 000 g/mol to 100 000 g/mol were prepared by dialysis through a cellulose bag with a cutoff of 14 000 g/mol. The dialyzed polymer was freeze-dried and redissolved in DI water to generate a 15 wt % stock solution. SiO_2 nanoparticles are LUDOX TM-50 colloidal silica (diameter 22 nm, 50 wt % suspension in water). Sodium chloride (NaCl) was purchased from Fisher Scientific and Sigma-Aldrich.

Solution Preparation. Stock solutions of 20 wt % dextran and 15 wt % PEG were prepared by stirring overnight with DI water. Solutions of PDADMAC and SiO_2 NPs suspensions were prepared by dilution of their respective stock solutions. The PDADMAC concentrations were adjusted to achieve isotonic conditions, with respect to the PEG/NP phase with 4 vol % of NP and 10 wt % PEG (Figure S1). Osmolality of solutions was measured by an Advanced Instruments Micro Osmometer Model 3300. The dex/PDADMAC stream contains 15 wt % dex/2 wt % nonfluorescent PDADMAC. The dex/fluo-PDADMAC stream has similar composition, with 25% vol. of the nonfluorescent PDADMAC replaced with fluo-PDADMAC. When adding salt to the complexing solutions, variations on the pH were observed. For the PEG/NP solution, increasing the NaCl concentration from 0 mM to 500 mM changed the pH of the solutions from ∼10 to 8.6. The dex/PDADMAC solution changed from 6.5 to 7.2 for the same NaCl concentration change.

Batch Membrane Growth. To study the growth of the membrane, large volumes (∼20 mL) of dextran/PDADMAC solution (1.5 wt % PDADMAC) and PEG/NP suspension (8% vol.) solutions were brought into a contact with each other. The membrane formation was achieved in two steps. First, a mixture of 10 wt % PEG, 8 vol % NP, 100 mM NaCl, and 15 wt % dextran was vortexed for 2 min and left to undergo phase separation in a 50 mL conical tube for 24 h. The PEG/NP phase segregated to the top and the dextran phase to the bottom (Figure S2). To initiate membrane growth, the lower phase was exchanged with a dex (15 wt %)/ PDADMAC (1.5 wt %) solution at 100 mM NaCl. This exchange was achieved by carefully inserting and withdrawing dextran phases at equal rates until the total lower phase volume was exchanged. After successful volume exchange, the interfacial growth was tracked at different intervals for 6 days.

Pendant Drop-Based Growth of Interfacial Membrane. Five milliliters of the continuous PEG/NP phase was placed in a 10 mL glass cuvette. To form the droplets, 1 μL of the dispersed (dex/PDADMAC (1.07 wt %)) was inserted into a continuous phase of PEG/NP at a flow rate of 1 μL/s. The syringe OD diameter was 0.90 mm (straight needle). Videos were recorded at 0.02 fps for 33 min.

Microfluidic Device Fabrication. A Y-junction microfluidic device was fabricated using traditional soft-lithography fabrication techniques. The device has 4 inlet ports which are connected to a rectangular channel with a width of 1 mm; two channels containing two phases meet at the Y-junction region which has the total width of 2 mm. The coflow region is 20 mm in length. The height of the device is 32 μm (Figure 4). To position the interface at the middle of the coflow region, the flow rates of two phases are tuned to match their shear stresses at the interface.[47] The flow rates were 3.5 μL/min for dex/PDADMAC at 100 mM NaCl and 19 μL/min for PEG/NP at 100 mM NaCl. More details are provided in the Supporting Information, Figure S8 and Table S1.

Thermogravimetric Analysis. An interfacial membrane for TGA was prepared by immersing a high concentration PDADMAC dextran

https://doi.org/10.1021/acsnano.2c08916
ACS Nano XXXX, XXX, XXX−XXX

stream (20 μL) into a bath of PEG/NP (3 to 4 mL). The dextran streak was placed on a SiO_2 wafer and left to undergo complexation for 1 day. The membrane was recovered in powder form (more details in Supporting Information) and used for the TGA analysis. The membrane was heated from room temperature (21 °C) to (800 °C) at 5 °C/min under nitrogen purge. The two isothermal stages are incorporated to promote water evaporation and to ensure complete thermal decomposition of the organic species.

Confocal Microscopy. Confocal imaging was performed on a Zeiss confocal microscope, with a 10× Zeiss objective and a laser excitation of 488 nm with an emission wavelength of 520−610 nm.

ASSOCIATED CONTENT

Supporting Information

The Supporting Information is available free of charge at https://pubs.acs.org/doi/10.1021/acsnano.2c08916.

Calibration curve for isotonic growth concentration; ATPS partition as a function of NaCl and SiO_2 NP; capsule formation at 0 mM NaCl; inverted pendant drop setups; schematic for sample preparation for TGA analysis, TGA of PDADMAC and PEG; transport of dextran, PDADMA and PEG in membrane formation, viscosity measurement of dex and PEG stream, and relevant flow rates, molecular weight characterization of filtered and fluorescent PDADMAC populations (PDF)

Movie S1: Growth of membrane at pendant drop at 100 mM NaCl droplet phase dextran/PDADMAC (AVI)

Movie S2: Growth of membrane at pendant drop at 100 mM NaCl droplet phase dextran/SiO_2 NP (AVI)

Movie S3: Growth of membrane at pendant drop at 100 mM NaCl droplet phase PEG/SiO_2 NP (AVI)

Movie S4: Growth of membrane at pendant drop at 500 mM NaCl droplet phase dextran/PDADMAC (AVI)

Movie S5: Growth of membrane at microfluidic y junction device single-insertion at 100 mM NaCl (AVI)

Movie S6: Growth of membrane at microfluidic y junction device single-insertion at 500 mM NaCl (AVI)

Movie S7: Sequential insertion at microfluidic y junction device at 0 mM NaCl (MP4)

Movie S8: Sequential insertion at microfluidic y junction device at 100 mM NaCl (MP4)

Movie S9: Sequential insertion at microfluidic y junction device at 500 mM NaCl (MP4)

AUTHOR INFORMATION

Corresponding Authors

Kathleen J. Stebe − *Department of Chemical and Biomolecular Engineering, University of Pennsylvania, Philadelphia, Pennsylvania 19104, United States;* orcid.org/0000-0003-0510-0513; Email: kstebe@seas.upenn.edu

Daeyeon Lee − *Department of Chemical and Biomolecular Engineering, University of Pennsylvania, Philadelphia, Pennsylvania 19104, United States;* orcid.org/0000-0001-6679-290X; Email: daeyeon@seas.upenn.edu

Author

Wilfredo Mendez-Ortiz − *Department of Chemical and Biomolecular Engineering, University of Pennsylvania, Philadelphia, Pennsylvania 19104, United States*

Complete contact information is available at: https://pubs.acs.org/10.1021/acsnano.2c08916

Author Contributions

Stebe, Lee, and Mendez all contributed to experimental design and interpretation of data. Mendez performed all experiments. All authors contributed to the writing of the manuscript. All authors have given approval to the final version of the manuscript.

Notes

The authors declare no competing financial interest.

ACKNOWLEDGMENTS

This material is based upon work supported by the National Science Foundation under Grant No. 1705891 and 1545884.

REFERENCES

(1) Becker, A. L.; Johnston, A. P. R.; Caruso, F. Layer-By-Layer-Assembled Capsules and Films for Therapeutic Delivery. *Small* **2010**, *6*, 1836−1852.

(2) Del Mercato, L. L.; Abbasi, A. Z.; Ochs, M.; Parak, W. J. Multiplexed Sensing of Ions with Barcoded Polyelectrolyte Capsules. *ACS Nano* **2011**, *5*, 9668−9674.

(3) Blaiszik, B. J.; Caruso, M. M.; McIlroy, D. A.; Moore, J. S.; White, S. R.; Sottos, N. R. Microcapsules Filled with Reactive Solutions for Self-Healing Materials. *Polymer (Guildf).* **2009**, *50*, 990−997.

(4) Kaufman, G.; Boltyanskiy, R.; Nejati, S.; Thiam, A. R.; Loewenberg, M.; Dufresne, E. R.; Osuji, C. O. Single-Step Microfluidic Fabrication of Soft Monodisperse Polyelectrolyte Microcapsules by Interfacial Complexation. *Lab Chip* **2014**, *14*, 3494−3497.

(5) Dupré De Baubigny, J.; Trégouët, C.; Salez, T.; Pantoustier, N.; Perrin, P.; Reyssat, M.; Monteux, C. One-Step Fabrication of PH-Responsive Membranes and Microcapsules through Interfacial H-Bond Polymer Complexation. *Sci. Rep.* **2017**, *7*, 1−7.

(6) Kim, M.; Yeo, S. J.; Highley, C. B.; Burdick, J. A.; Yoo, P. J.; Doh, J.; Lee, D. One-Step Generation of Multifunctional Polyelectrolyte Microcapsules via Nanoscale Interfacial Complexation in Emulsion (NICE). *ACS Nano* **2015**, *9*, 8269−8278.

(7) Wu, X.; Yuan, Q.; Liu, S.; Shi, S.; Russell, T. P.; Wang, D. Nanorod-surfactant Assemblies and Their Interfacial Behavior at Liquid-liquid Interfaces. *ACS Macro Lett.* **2019**, *8*, 512−518.

(8) Xu, R.; Liu, T.; Sun, H.; Wang, B.; Shi, S.; Russell, T. P. Interfacial Assembly and Jamming of Polyelectrolyte Surfactants: A Simple Route to Print Liquids in Low-Viscosity Solution. *ACS Appl. Mater. Interfaces* **2020**, *12*, 18116−18122.

(9) Cacace, D. N.; Rowland, A. T.; Stapleton, J. J.; Dewey, D. C.; Keating, C. D. Aqueous Emulsion Droplets Stabilized by Lipid Vesicles as Microcompartments for Biomimetic Mineralization. *Langmuir* **2015**, *31*, 11329−11338.

(10) Hann, S. D.; Niepa, T. H. R.; Stebe, K. J.; Lee, D. One-Step Generation of Cell-Encapsulating Compartments via Polyelectrolyte Complexation in an Aqueous Two Phase System. *ACS Appl. Mater. Interfaces* **2016**, *8*, 25603−25611.

(11) Pir Cakmak, F.; Keating, C. D. Combining Catalytic Microparticles with Droplets Formed by Phase Coexistence: Adsorption and Activity of Natural Clays at the Aqueous/Aqueous Interface. *Sci. Rep.* **2017**, *7*, 1−14.

(12) Inostroza-Brito, K. E.; Collin, E.; Siton-Mendelson, O.; Smith, K. H.; Monge-Marcet, A.; Ferreira, D. S.; Rodríguez, R. P.; Alonso, M.; Rodríguez-Cabello, J. C.; Reis, R. L.; Sagués, F.; Botto, L.; Bitton, R.; Azevedo, H. S.; Mata, A. Co-Assembly, Spatiotemporal Control and Morphogenesis of a Hybrid Protein-Peptide System. *Nat. Chem.* **2015**, *7*, 897−904.

(13) Hann, S. D.; Lee, D.; Stebe, K. J. Tuning Interfacial Complexation in Aqueous Two Phase Systems with Polyelectrolytes and Nanoparticles for Compound All Water Emulsion Bodies (AWE-Somes). *Phys. Chem. Chem. Phys.* **2017**, *19*, 23825−23831.

(14) Capito, R. M.; Azevedo, H. S.; Velichko, Y. S.; Mata, A.; Stupp, S. I. Self-Assembly of Large and Small Molecules into Hierarchically Ordered Sacs and Membranes. *Science (80-.).* **2008**, *319*, 1812−1816.
(15) Mendoza-Meinhardt, A.; Botto, L.; Mata, A. A Fluidic Device for the Controlled Formation and Real-Time Monitoring of Soft Membranes Self-Assembled at Liquid Interfaces. *Sci. Rep.* **2018**, *8*, 1−9.
(16) Ma, Q.; Song, Y.; Kim, J. W.; Choi, H. S.; Shum, H. C. Affinity Partitioning-Induced Self-Assembly in Aqueous Two-Phase Systems: Templating for Polyelectrolyte Microcapsules. *ACS Macro Lett.* **2016**, *5*, 666−670.
(17) Ma, Q.; Yuan, H.; Song, Y.; Chao, Y.; Mak, S. Y.; Shum, H. C. Partitioning-Dependent Conversion of Polyelectrolyte Assemblies in an Aqueous Two-Phase System. *Soft Matter* **2018**, *14*, 1552−1558.
(18) Song, Y.; Chan, Y. K.; Ma, Q.; Liu, Z.; Shum, H. C. All-Aqueous Electrosprayed Emulsion for Templated Fabrication of Cytocompatible Microcapsules. *ACS Appl. Mater. Interfaces* **2015**, *7*, 13925−13933.
(19) Hann, S. D.; Stebe, K. J.; Lee, D. All-Aqueous Assemblies via Interfacial Complexation: Toward Artificial Cell and Microniche Development. *Langmuir* **2017**, *33*, 10107−10117.
(20) Xie, G.; Forth, J.; Chai, Y.; Ashby, P. D.; Helms, B. A.; Russell, T. P. Compartmentalized, All-Aqueous Flow-Through-Coordinated Reaction Systems. *Chem.* **2019**, *5*, 2678−2690.
(21) Gonçalves, R. C.; Vilabril, S.; Neves, C. M. S. S.; Freire, M. G.; Coutinho, J. A. P.; Oliveira, M. B.; Mano, J. F. All-Aqueous Freeform Fabrication of Perfusable Self-Standing Soft Compartments. *Adv. Mater.* **2022**, *34*, 2200352.
(22) Lin, D.; Liu, T.; Yuan, Q.; Yang, H.; Ma, H.; Shi, S.; Wang, D.; Russell, T. P. Stabilizing Aqueous Three-Dimensional Printed Constructs Using Chitosan-Cellulose Nanocrystal Assemblies. *ACS Appl. Mater. Interfaces* **2020**, *12*, 55426−55433.
(23) Hann, S. D.; Stebe, K. J.; Lee, D. AWE-Somes: All Water Emulsion Bodies with Permeable Shells and Selective Compartments. *ACS Appl. Mater. Interfaces* **2017**, *9*, 25023−25028.
(24) Yin, Y.; Liu, T.; Wang, B.; Yin, B.; Yang, Y.; Russell, T. P.; Shi, S. Nanoparticle/Polyelectrolyte Complexes for Biomimetic Constructs. *Adv. Funct. Mater.* **2022**, *32*, 2108895.
(25) Guzmán, E.; Ritacco, H.; Rubio, J. E. F.; Rubio, R. G.; Ortega, F. Salt-Induced Changes in the Growth of Polyelectrolyte Layers of Poly(Diallyl-Dimethylammonium Chloride) and Poly(4-Styrene Sulfonate of Sodium). *Soft Matter* **2009**, *5*, 2130−2142.
(26) Fares, H. M.; Schlenoff, J. B. Diffusion of Sites versus Polymers in Polyelectrolyte Complexes and Multilayers. *J. Am. Chem. Soc.* **2017**, *139*, 14656−14667.
(27) Picart, C.; Mutterer, J.; Richert, L.; Luo, Y.; Prestwich, G. D.; Schaaf, P.; Voegel, J. C.; Lavalle, P. Molecular Basis for the Explanation of the Exponential Growth of Polyelectrolyte Multilayers. *Proc. Natl. Acad. Sci. U. S. A.* **2002**, *99*, 12531−12535.
(28) Diamond, A.; Hsu, J. Phase Diagrams for Dextran-PEG Aquoeous Two-Phase Systems at 22°C. *Biotechnol. Technol.* **1989**, *3*, 119−124.
(29) Chao, Y.; Shum, H. C. Emerging Aqueous Two-Phase Systems: From Fundamentals of Interfaces to Biomedical Applications. *Chem. Soc. Rev.* **2020**, *49*, 114−142.
(30) Rose, K. A.; Lee, D.; Composto, R. J. PH-Mediated Nanoparticle Dynamics in Hydrogel Nanocomposites. *Soft Matter* **2021**, *17*, 2765−2774.
(31) Zeng, X.; Osseo-Asare, K. Partitioning Behavior of Silica in the PEG/Dextran/H2O Aqueous Biphasic System. *Colloids Surfaces A Physicochem. Eng. Asp.* **2003**, *226*, 45−54.
(32) Rubio, J.; Kitchener, J. A. The Mechanism of Adsorption of Poly(Ethylene Oxide) Flocculant on Silica. *J. Colloid Interface Sci.* **1976**, *57*, 132−142.
(33) Iler, R. K. Hydrogen-Bonded Complexes of Silica with Organic Compounds. In *Biochemistry of Silicon and Related Problems*, Bendz, G.; Lindqvist, I.; Runnström-Reio, V., Eds.; Springer US: Boston, MA, 1978; pp 53−76.
(34) Baudin, I.; Ricard, A.; Audebert, R. Adsorption of Dextrans and Pullulans at the Silica-Water Interface; Hydrodynamic Layer Thickness Measurements; Role in the Fouling of Ultrafiltration Membranes. *J. Colloid Interface Sci.* **1990**, *138*, 324−331.
(35) Jucker, B. A.; Harms, H.; Hug, S. J.; Zehnder, A. J. B. Adsorption of Bacterial Surface Polysaccharides on Mineral Oxides Is Mediated by Hydrogen Bonds. *Colloids Surfaces B Biointerfaces* **1997**, *9*, 331−343.
(36) Dupré De Baubigny, J.; Perrin, P.; Pantoustier, N.; Salez, T.; Reyssat, M.; Monteux, C. Growth Mechanism of Polymer Membranes Obtained by H-Bonding across Immiscible Liquid Interfaces. *ACS Macro Lett.* **2021**, *10*, 204−209.
(37) Gunes, D. Z.; Pouzot, M.; Rouvet, M.; Ulrich, S.; Mezzenga, R. Tuneable Thickness Barriers for Composite o/w and w/o Capsules, Films and Their Decoration with Particles. *Soft Matter* **2011**, *7*, 9206−9215.
(38) Dautzenberg, H.; Görnitz, E.; Jaeger, W. Synthesis and Characterization of Poly(Diallyldimethylammonium Chloride) in a Broad Range of Molecular Weight. *Macromol. Chem. Phys.* **1998**, *199*, 1561−1571.
(39) Fares, H. M.; Wang, Q.; Yang, M.; Schlenoff, J. B. Swelling and Inflation in Polyelectrolyte Complexes. *Macromolecules* **2019**, *52* (52), 610−619.
(40) Jomaa, H. W.; Schlenoff, J. B. Salt-Induced Polyelectrolyte Interdiffusion in Multilayered Films: A Neutron Reflectivity Study. *Macromolecules* **2005**, *38*, 8473−8480.
(41) Dautzenberg, H.; Arnold, G.; Tiersch, B.; Lukanoff, B.; Eckert, U. Polyelectrolytes Complex Formation at the Interface of Solutions. *Prog. Colloid Polym. Sci.* **1996**, *101*, 149−156.
(42) Fu, J.; Schlenoff, J. B. Driving Forces for Oppositely Charged Polyion Association in Aqueous Solutions: Enthalpic, Entropic, but Not Electrostatic. *J. Am. Chem. Soc.* **2016**, *138*, 980−990.
(43) Chang, L. W.; Lytle, T. K.; Radhakrishna, M.; Madinya, J. J.; Vélez, J.; Sing, C. E.; Perry, S. L. Sequence and Entropy-Based Control of Complex Coacervates. *Nat. Commun.* **2017**, *8*, 1−7.
(44) Dubas, S. T.; Schlenoff, J. B. Swelling and Smoothing of Polyelectrolyte Multilayers by Salt. *Langmuir* **2001**, *17*, 7725−7727.
(45) Pham, P.; Vo, T.; Luo, X. Steering Air Bubbles with an Add-on Vacuum Layer for Biopolymer Membrane Biofabrication in PDMS Microfluidics. *Lab Chip* **2017**, *17*, 248−255.
(46) Jia, N.; Rosella, E.; Juère, E.; Pouliot, R.; Kleitz, F.; Greener, J. A Microfluidic Approach to Micromembrane Synthesis for Complex Release Profiles of Nanocarriers. *Lab Chip* **2020**, *20*, 1066−1071.
(47) Rosella, E.; Jia, N.; Mantovani, D.; Greener, J. A Microfluidic Approach for Development of Hybrid Collagen-Chitosan Extracellular Matrix-like Membranes for on-Chip Cell Cultures. *J. Mater. Sci. Technol.* **2021**, *63*, 54−61.

https://doi.org/10.1021/acsnano.2c08916
ACS Nano XXXX, XXX, XXX−XXX